

# Fastest first-passage time for multiple searchers with finite speed

Denis S. Grebenkov,<sup>1</sup> Ralf Metzler,<sup>2</sup> and Gleb Oshanin<sup>3</sup>

<sup>1</sup>*Laboratoire de Physique de la Matière Condensée (UMR 7643), CNRS – Ecole Polytechnique, IP Paris, 91120 Palaiseau, France*

<sup>2</sup>*Institute of Physics & Astronomy, University of Potsdam, 14476 Potsdam-Golm, Germany*

<sup>3</sup>*Sorbonne Université, CNRS, Laboratoire de Physique Théorique de la Matière Condensée (UMR CNRS 7600), 4 Place Jussieu, 75252 Paris Cedex 05, France*

(Dated: February 18, 2026)

We study analytically and numerically the mean fastest first-passage time (FFPT) to an immobile target for an ensemble of  $N$  independent finite-speed random searchers driven by dichotomous noise and described by the telegrapher's equation. In stark contrast to the well-studied case of Brownian particles—for which the mean FFPT vanishes logarithmically with  $N$ —we uncover that the mean FFPT is bounded from below by the minimal ballistic travel time, with an exponentially fast convergence to this bound as  $N \rightarrow \infty$ . This behavior reveals a dramatic efficiency advantage of physically realistic, finite-speed searchers over Brownian ones and illustrates how diffusive macroscopic models may be conceptually misleading in predicting the short-time behavior of a physical system. We extend our analysis to anomalous diffusion generated by Riemann-Liouville-type dichotomous noises and find that target detection is more efficient in the superdiffusive regime, followed by normal and then subdiffusive regimes, in agreement with physical intuition and contrary to earlier predictions.

In many biological contexts, diverse agents must efficiently locate distant targets—such as transcription factors binding to specific operators on the cellular DNA, immune cells detecting pathogens, or signaling molecules reaching their conjugate receptors [1–3]. These processes are inherently stochastic and often proceed in crowded dynamic environments such as cellular cytoplasm. Although the first-passage statistics for individual searchers are quite well understood [4–6], biological systems rarely rely on a single agent; instead, multiple searchers are deployed in parallel to speed up target detection [2, 7, 8].

When  $N$  searchers begin simultaneously, target detection is determined not by a single agent's shortest arrival time  $\tau$ , but competitively by the earliest arrival time among all searchers. The problem thus shifts from individual first-passage times  $\tau_k$ ,  $k = 1, 2, \dots, N$ , to the statistic of the extremal random variable  $\mathcal{T}_N = \min\{\tau_1, \dots, \tau_N\}$ —the fastest first-passage time (FFPT). Order statistics therefore play a central role: the key aspects are the FFPT distribution and how its moments scale with  $N$ , characterizing the efficiency of such a multi-agent search. The analysis of such multiple searcher dynamics reveals how redundancy improves both the reliability and speed of biological search, offering insight into how living systems may optimize their performance.

Most existing analyses of multi-agent search assume that all agents start from the same point simultaneously and move independently as Brownian walkers with the same diffusion coefficient  $D$  [9–16]. Their positions follow Langevin dynamics with Gaussian white noise, and the position probability density function (PDF) of each searcher evolves according to the diffusion equation from  $t = 0$ , a framework that accurately captures the long-time behavior of many stochastic processes in nature. Within this setting, the *mean* FFPT to a target at a dis-

tance  $x_0$  follows the inverse-logarithmic law [9–16]

$$\overline{\mathcal{T}_N} \simeq \frac{x_0^2}{4D \ln(N)} \quad (N \rightarrow \infty). \quad (1)$$

Here the bar denotes averaging with respect to individual trajectory realizations of all searchers, and the symbol “ $\simeq$ ” signifies that we consider solely the leading-order behavior in the limit  $N \rightarrow \infty$ . This result was first derived for one-dimensional continuous-space systems, but later shown to hold in bounded domains of any dimension [17, 18], because it is dominated by so-called “direct” trajectories [19, 20] that go straight to the target, rendering the actual embedding spatial dimension irrelevant.

The asymptotic form (1) shows that deploying more and more searchers steadily lowers the mean FFPT, albeit only logarithmically with  $N$ . In the limit  $N \rightarrow \infty$ , the fastest searcher would thus reach the distant target arbitrarily quickly—effectively instantaneously. Moreover, assuming that the agents undergo a subdiffusive motion with the mean-squared displacement (MSD)  $x^2(t) \propto t^\alpha$  ( $0 < \alpha < 1$ ) and a position PDF obeying a fractional diffusion equation [21], it was shown that

$$\overline{\mathcal{T}_N} \simeq \frac{t_\alpha}{[\ln(N)]^{\frac{2}{\alpha}-1}} \quad (N \rightarrow \infty), \quad (2)$$

where  $t_\alpha$  is a characteristic time-scale [22]. This asymptotic result indicates that for subdiffusive dynamics,  $\overline{\mathcal{T}_N}$  also vanishes as  $N \rightarrow \infty$ . Strikingly, Eq. (2) implies that  $\overline{\mathcal{T}_N} \rightarrow 0$  when  $\alpha \rightarrow 0$ , suggesting that *slower* diffusion *enhances* the speed of the fastest arrival, as highlighted in the title of [22]. Although mathematically rigorous, the results (1) and (2) are clearly unrealistic—even the fastest searcher needs a finite time to reach a target a finite distance away—thus underscoring the need for a more refined analysis that yields more plausible behavior.

Here, we revisit this long-standing problem by assuming that individual searchers follow a one-dimensional generalized Langevin dynamics driven by symmetric *dichotomous* noise—a stochastic motion with random switching between velocities  $\pm v$  with rate  $\lambda$  [23, 24] (see also [25, 26] and references therein). This choice avoids the unphysical behavior inherent in Gaussian white-noise models, where a searcher has a non-zero probability of appearing arbitrarily far from its starting point in arbitrarily short time, allowing for unrealistically small first-passage times (historically, this problem is well known in heat transport, where it is circumvented by replacing the parabolic diffusion equation by a hyperbolic Cattaneo equation with finite propagation speed [27, 28]). For large  $N$ , such short-time artifacts dominate the moments of  $\mathcal{T}_N$ , over-estimating the survival probabilities. Dichotomous noise thus provides a more realistic framework to capture the short-time dynamics relevant to multi-agent search. Moreover, symmetric dichotomous noise with alternating velocities naturally encodes strong antipersistence—common in crowded environments—since each forward step is followed by a backward one (see, e.g., [29]). We also note that this very framework has been successfully used to model bacterial and other active-particle dynamics, yielding physically realistic behavior (see, e.g., [30–32]). Particularly, the motion of sperm cells, one of the major biological motivations for studying the mean ffPFT [11, 16], would be more naturally described by (biased) dichotomous noises than by white Gaussian ones.

We show that the dichotomous-noise framework naturally removes the above unphysical artifacts and provides a more physically realistic and consistent behavior of the mean ffPFT  $\overline{\mathcal{T}}_N$ . Within this picture,  $\overline{\mathcal{T}}_N$  tends to  $t_{\min} = x_0/v$  as  $N \rightarrow \infty$ —the ballistic travel time and hence the natural lower bound on  $\overline{\mathcal{T}}_N$ . The convergence to this value with increasing  $N$  is entirely controlled by the key parameter, the dimensionless ballistic travel time number  $\gamma = x_0\lambda/v$ . The parameter  $\gamma$  can be quite small for particles moving in viscoelastic media such as the cell cytoplasm, or for bacteria. Conversely, it may attain large values for particles moving in aqueous solutions. We show below that  $\gamma$  determines the characteristic number  $N_\gamma$  that separates two asymptotic regimes: For  $N \gg N_\gamma$ , the approach of  $\overline{\mathcal{T}}_N$  to  $t_{\min}$  is described by an exponential function of  $N$ ,  $\overline{\mathcal{T}}_N - t_{\min} \propto e^{-N/N_\gamma}$ , which signifies that deploying  $N$  searchers may actually be, by far, a more efficient strategy than one might expect from the logarithmic reduction predicted by Eqs. (1) and (2). In contrast, for  $N$  in the interval  $3 \leq N \ll N_\gamma$ , the approach is quite slow and for  $\gamma \rightarrow \infty$  (and hence  $N_\gamma \rightarrow \infty$ ) becomes consistent with the dependence in Eq. (1). Concurrently, the result in Eq. (1) follows directly from our analysis if we first take the "diffusion limit" of the dichotomous noise and then consider the limit  $N \rightarrow \infty$ , which demonstrates that these limits do not commute. To probe the behavior of  $\overline{\mathcal{T}}_N$  for *anomalous* diffusion, we consider the dynamics driven by the Riemann-Liouville fractional dichotomous

noise [33]. We show that also in this case the mean ffPFT tends to some minimal travel time (see Eq. (16) below) in the limit  $N \rightarrow \infty$  and, for physically relevant parameters, the approach is faster in the superdiffusive regime than in the diffusive one, and the latter outperforms subdiffusion, which is an intuitively expected and correct trend, as compared to the one predicted by Eq. (2).

*Model.* Consider a one-dimensional system in which  $N$  particles are released from a point  $x_0 > 0$  at time  $t = 0$  and search for an immobile target at the origin. All  $N$  particles move on the positive halfline independently of each other, and their instantaneous positions  $x_k(t)$ ,  $k = 1, 2, \dots, N$ , obey the stochastic differential equations

$$\dot{x}_k(t) = \eta_k(t), \quad x_k(0) = x_0, \quad (3)$$

where  $\eta_k(t)$  are statistically-independent *symmetric* dichotomous noises alternating between the values  $\pm v$ . The switching events occur after random, exponentially distributed time intervals with the rate  $\lambda$ . The mean and autocovariance function of the noises read [23, 24]

$$\overline{\eta_k(t)} = 0, \quad \overline{\eta_k(t)\eta_{k'}(t')} = \delta_{k,k'} 2\lambda D e^{-2\lambda|t-t'|}, \quad (4)$$

in terms of the Kronecker-delta  $\delta_{k,k'}$  and the long-time diffusion coefficient  $D = v^2/(2\lambda)$ . Here  $1/(2\lambda)$  is a finite correlation time of the noises. The MSD of  $x_k(t)$  scales linearly with time in the long-time limit. Based on this model we focus on the statistics of the first-passage times  $\tau_k$  to the target of the respective searchers and on the above-defined extremal random variable  $\overline{\mathcal{T}}_N$ , the ffPFT.

We also study dichotomous dynamics in a broader context by extending it to anomalous diffusion—processes characterized by an anomalous diffusion exponent  $\alpha$  that may be less than unity (subdiffusion) or greater than unity (superdiffusion) [21]. We model anomalous diffusion by a Riemann-Liouville-type fractional dichotomous process as introduced in [33], in which individual searcher trajectories are described by the stochastic integral

$$x_k(t) = x_0 + \int_0^t K(t-t')\eta_k(t')dt', \quad (5)$$

$$K(t) = (t/T_0)^{(\alpha-1)/2}/\Gamma((\alpha+1)/2), \quad 0 < \alpha < 2,$$

where  $T_0$  is a characteristic time-scale of the power-law memory kernel  $K(t)$ . The MSD of such a process grows with time as  $x^2(t) \propto t^\alpha$ , in analogy to the fractional dynamics studied in [22]. Note that the centered process  $y_k(t) = x_k(t) - x_0$  evolves inside the "light cone"  $|y_k(t)| \leq y^*(t)$  for any  $t$ , where  $y^*(t) \sim vT_0(t/T_0)^{(1+\alpha)/2}$ . The position PDF of  $y_k(t)$ , which is supported on  $[-y^*(t), y^*(t)]$  and vanishes outside of this support, was studied in detail in [33]. The PDF is approximately Gaussian in its central part and vanishes at the endpoints  $\pm y^*(t)$  of the support. For this model we will also study the statistics of the first-passage times and the mean ffPFT by extensive numerical simulations.

*Central results.* The PDF of first-passage times for a single particle moving randomly subject to a symmetric

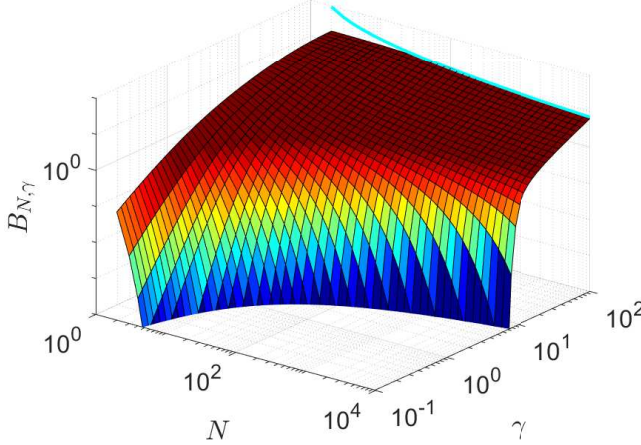


FIG. 1. (Color online) 3D plot of  $B_{N,\gamma}$  obtained from numerical evaluation of the integrals in Eqs. (7a) and (7b), as function of  $N$  and  $\gamma$ . The cyan solid line indicates our asymptotic large- $\gamma$  prediction  $2\gamma/(\pi \ln N)$ , see Eqs. (11) and (13).

dichotomous noise was analyzed in [34] (see also [35, 36]). For completeness, a derivation is presented in the Supplemental Material (SM), Sec. A [37]. Our main goal here is to determine the mean ffPT  $\bar{T}_N$  and to study its functional dependence on  $N$  and  $\gamma$ . Relegating details of calculations to SM.B1 [37], we find that for arbitrary  $N \geq 3$  and  $\gamma > 0$ ,

$$\bar{T}_N = t_{\min}(1 + B_{N,\gamma}), \quad t_{\min} = x_0/v, \quad (6)$$

where  $t_{\min}$  is the ballistic travel time, and the dimensionless function  $B_{N,\gamma}$  quantifies the relative excess induced by the dichotomous dynamics of  $N$  searchers,

$$B_{N,\gamma} = \int_1^\infty [f_\gamma(y)]^N dy, \quad (7a)$$

$$f_\gamma(y) = \gamma \int_{\text{arccosh}(y)}^\infty e^{-\gamma \cosh z} I_1(\gamma \sinh z) dz, \quad (7b)$$

where  $I_1(z)$  is the modified Bessel function of the first kind and  $\gamma$  the above-mentioned dimensionless number  $\gamma = x_0 \lambda / v = vx_0 / (2D)$ . Note that  $B_{N,\gamma} \geq 0$  so that  $\bar{T}_N$  cannot become smaller than  $t_{\min}$ , i.e.,  $t_{\min}$  is a natural lower bound on the mean ffPT. Furthermore,  $B_{N,\gamma}$  is a monotonically *increasing* function of  $\gamma$  and a monotonically *decreasing* function of  $N$ , as intuitively expected. In Fig. 1 we plot  $B_{N,\gamma}$  obtained from numerical evaluation of the integrals in Eqs. (7a) and (7b), which illustrates its overall behavior and clearly highlights these features.

Before we discuss the asymptotic behavior of expression (6), we consider an "order of magnitude" estimate of  $\gamma$  for several physical systems. For instance, the diffusive dynamics of a small protein or of an ion, say  $K^+$ , in water, has a noise correlation time of the order of picoseconds,  $(2\lambda)^{-1} \sim 10^{-12}$  s. The diffusion coefficients of a small protein or of an ion are of the order

of  $10^2 \mu\text{m}^2/\text{s}$  [38] and  $10^3 \mu\text{m}^2/\text{s}$  [39], respectively, such that  $\gamma \sim 10^4 x_0 / \mu\text{m}$  or even  $\gamma \sim 10^5 x_0 / \mu\text{m}$ . For  $x_0$  of the order of a few micrometers,  $\gamma$  is therefore very large. In turn, in a crowded environment, e.g., the cellular cytoplasm, the correlation time of noise is much longer:  $(2\lambda)^{-1}$  typically ranges from milliseconds to seconds [40, 41]. Concurrently, the diffusion coefficient of a small protein in cytoplasm is typically suppressed by more than an order of magnitude compared to water [42] and the ionic diffusion is reduced by a factor of a few [39]. Respectively, one finds  $\gamma \sim (1-10) x_0 / \mu\text{m}$ . Again, for  $x_0$  in the range of a few micrometers,  $\gamma$  should attain in this physical situation very modest values. Lastly, consider the dynamics of bacteria such as *E. coli*, which performs paradigmatic run-and-tumble motion [30, 31]. A systematic analysis of the experimental data has been recently performed in [32], giving  $D \approx 0.3 \mu\text{m}^2/\text{s}$ ,  $v \approx 17 \mu\text{m/s}$  and the mean run time of order of 3 s. This leads to  $\gamma \approx 0.5 x_0 / \mu\text{m}$ , and hence, for a target site placed at a distance of a few micrometers away,  $\gamma$  amounts to several units. Therefore, all values of  $\gamma$  are in principle relevant but correspond to specific physical situations: while  $\gamma$  can be large for the dynamics in aqueous solutions, moderate or even relatively small values correspond to the motion of bacteria, or ions and small proteins in cellular cytoplasm.

*Asymptotic large- $N$  form of  $B_{N,\gamma}$ .* We first consider the regime when  $\gamma$  is fixed and  $N \gg N_\gamma$ , where

$$N_\gamma = -1 / \ln(1 - e^{-\gamma}), \quad (8)$$

a crucial parameter setting the scale for the number of searchers beyond which the exponential decay becomes relevant. We show in SM.B2 [37] that in this regime

$$B_{N,\gamma} \approx 2(e^\gamma - 1)(\gamma^2 N)^{-1} e^{-N/N_\gamma} \quad (N \gg N_\gamma), \quad (9)$$

which demonstrates that the large- $N$  decay of  $B_{N,\gamma}$  is always *exponential*, in striking contrast with the prediction in Eq. (1) for Brownian walkers. In Fig. 2, we depict the asymptotic form in Eq. (9) for different values of  $\gamma$  together with the corresponding values of  $N_\gamma$  (crosses and vertical dashed lines), alongside with numerical evaluations of the integrals in Eqs. (7a) and (7b) (colored solid, dashed and dot-dashed curves). We observe excellent agreement between our prediction in Eq. (9) and the numerical evaluation of the excess factor  $B_{N,\gamma}$ .

*Intermediate- $N$  form of  $B_{N,\gamma}$ .* By virtue of Eq. (8), the threshold value is  $N_\gamma \approx e^\gamma$  for large  $\gamma$ , so that the range in which the large- $N$  exponential behavior can be observed shifts to extremely large (and even unphysical) values of  $N$ . Indeed, while  $N_\gamma$  has quite modest values for small  $\gamma$  (e.g.,  $N_\gamma \approx 2.18$  for  $\gamma = 1$ ,  $N_\gamma \approx 6.88$  for  $\gamma = 2$  and  $N_\gamma \approx 148$  for  $\gamma = 5$ ), already for  $\gamma = 26$  it exceeds  $10^{11}$ , beyond practically realizable numbers of deployed searchers. Therefore, the intermediate- $N$  regime  $3 \leq N \ll N_\gamma$  is a physically relevant domain for systems in which  $\gamma$  is large, e.g., in aqueous solutions.

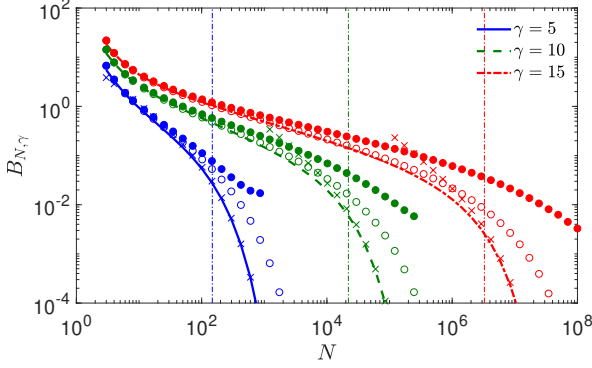


FIG. 2. (Color online) Excess factor  $B_{N,\gamma}$  for  $\gamma = 5$  (blue),  $\gamma = 10$  (green) and  $\gamma = 15$  (red) as function of  $N$ . Colored solid, dashed and dot-dashed curves depict the corresponding factors  $B_{N,\gamma}$  obtained by a numerical evaluation of the integrals in Eqs. (7a) and (7b). Crosses present the large- $N$  asymptotic form in Eq. (9). Empty colored circles show the intermediate- $N$  asymptotic form in Eq. (10), whereas the filled circles indicate the asymptotic relation (11). Colored vertical thin dash-dotted lines represent  $N_\gamma \approx 148$ ,  $N_\gamma \approx 2.2 \times 10^4$  and  $N_\gamma \approx 3.3 \times 10^6$ , respectively.

The asymptotic analysis in this regime is much subtler. In SM.B3 [37], we show that  $B_{N,\gamma}$  can be accurately approximated in this  $N$ -range as

$$B_{N,\gamma} \approx \int_0^1 \frac{1-x^4}{x^3} [\text{erf}(\sqrt{\gamma}x)]^N dx, \quad (10)$$

where  $\text{erf}(x)$  is the error function. In Fig. 2 we depict the approximate form (10) by empty colored circles, confronting this prediction with the numerically evaluated integrals in Eqs. (7a) and (7b). We observe perfect agreement over an extended range of  $N$ , which broadens progressively as  $\gamma$  increases. Furthermore, using the tight upper bound on  $\text{erf}(x)$  [43] and assuming that  $N$  is even, we find the following asymptotic relation which holds uniformly for any  $N$  within the interval  $3 \leq N \ll N_\gamma$ ,

$$B_{N,\gamma} \approx \frac{2\gamma}{\pi} S_{N/2} - 1 + \frac{\pi}{8\gamma} H_{N/2} + \mathcal{O}(e^{-\gamma}), \quad (11)$$

where  $H_n = \sum_{j=1}^n 1/j$  is the harmonic number, and

$$S_n = \sum_{j=1}^n (-1)^j \binom{n}{j} j \ln(j). \quad (12)$$

The above result is presented in Fig. 2 by filled colored circles and shows that Eq. (11) provides an accurate approximation of the behavior of the excess factor  $B_{N,\gamma}$  for intermediate values of  $N$ . In the limit  $\gamma \rightarrow \infty$ , one has  $N_\gamma \rightarrow \infty$ , and we may consider the asymptotic behavior of  $B_{N,\gamma}$  when  $N \rightarrow \infty$ . In this limit the dominant contribution to  $B_{N,\gamma}$  in Eq. (11) comes from the first term proportional to  $\gamma$ . Taking into account that (see SM.B3

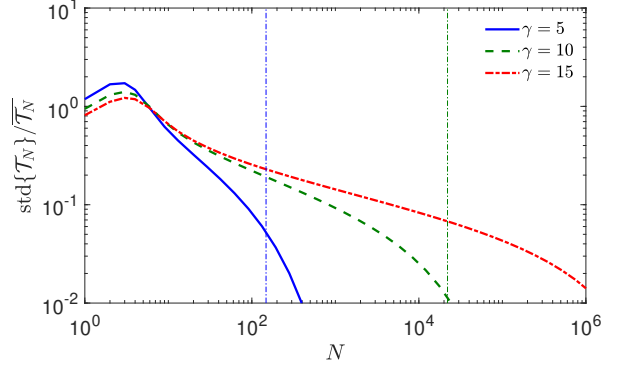


FIG. 3. (Color online) Coefficient of variation  $\kappa$  from Eq. (14) as function of  $N$  for three values of  $\gamma$ .

[37])

$$S_{N/2} \simeq \frac{1}{\ln(N/2)} - \frac{C}{\ln^2(N/2)} + \frac{C^2 + \pi^2/6}{\ln^3(N/2)}, \quad (13)$$

where  $C = 0.577..$  is the Euler-Mascheroni constant, and using Eqs. (11) and (6), we find that, to leading order in  $N$ ,  $\overline{\mathcal{T}_N} \simeq x_0^2/(\pi D \ln N)$ . This expression agrees with Eq. (1) for Brownian walkers apart from the numerical factor  $(1/\pi)$  instead of  $(1/4)$ . The function  $2\gamma/(\pi \ln(N))$  is depicted by the thick solid line in Fig. 1 showing a very good agreement with the numerically evaluated  $B_{N,\gamma}$ . For a discussion of how one recovers Eq. (1) as the diffusion limit of the dichotomous noise, see SM.B4 [37].

It is legitimate to ask whether the mean fFPT is representative of the actual behavior. To provide an answer, we consider the coefficient of variation  $\kappa$  of the fFPT, defined as the ratio of the standard deviation of the realization-dependent fFPT divided by its mean,

$$\kappa = \frac{\sqrt{\overline{\mathcal{T}_N^2} - \overline{\mathcal{T}_N}^2}}{\overline{\mathcal{T}_N}}. \quad (14)$$

This quantity is illustrated in Fig. 3, where  $\kappa$  is shown as function of  $N$  for three values of  $\gamma$ . We find that  $\kappa$  exceeds unity only when a small number of searchers is deployed, which is intuitively expected. For larger  $N$ , however,  $\kappa$  drops sharply below unity, indicating that fluctuations of the fFPT become negligible and that the arrival times of the searchers concentrate around the common value  $t_{\min}$ : the mean fFPT provides a faithful characterization of the search dynamics. In fact, in the regime  $N \gg N_\gamma$ , we find (see SM.B5 [37]) that  $\kappa$  decays *exponentially* with  $N$ ,

$$\kappa \approx \frac{2\sqrt{2}(e^\gamma - 1)}{\gamma^2 N} e^{-N/(2N_\gamma)}. \quad (15)$$

*Anomalous diffusion.* In contrast to Brownian motion, anomalous diffusion is not universal in the sense that many physically different stochastic processes give rise to the MSD-scaling  $x^2(t) \propto t^\alpha$  [21, 44, 45]. A flexible

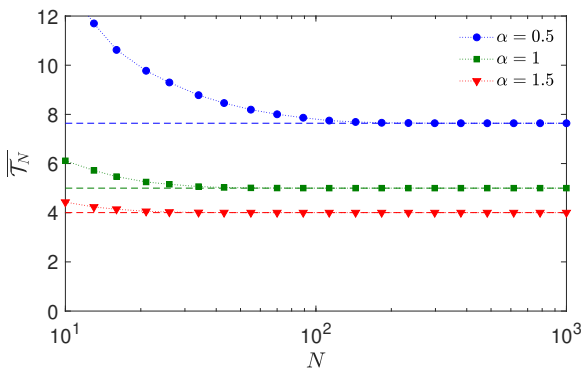


FIG. 4. Mean fFPT  $\overline{T_N}$  as a function of  $N$  for the dynamics generated by Riemann-Liouville dichotomous noise for three values of the scaling exponent:  $\alpha = 0.5$  (subdiffusive behavior, blue),  $\alpha = 1$  (diffusive behavior, green) and  $\alpha = 1.5$  (superdiffusive behavior, red). The symbols depict the results of simulations with  $M = 10^4$  particles, for  $T_0 = 1$ ,  $D = 1$ ,  $v = 1$ ,  $\lambda = v^2/(2D)$ , and  $x_0 = 5$  (such that  $x_0/(vT_0) > 1$ ). The horizontal dashed lines indicate the corresponding ballistic travel times in Eq. (16).

prototype process is Riemann-Liouville fractional Brownian motion, a variant of Mandelbrot-van Ness fractional Brownian motion [46, 47, 49] based on fractional Gaussian noise. Fractional Brownian motion has been shown to provide good quantitative descriptions of anomalous-diffusive motion in a variety of viscoelastic media and even for animal motion [48] (and references therein).

We consider a Riemann-Liouville fractional dichotomous process [33], which preserves the essential property of finite-speed propagation. This is a convenient unifying framework to illustrate the consequences for the search efficiency in the  $N$ -searcher case. When a typical searcher performs many jumps before reaching the target and the timescale  $T_0$  of the memory kernel is sufficiently small to ensure  $x_0/(vT_0) > 1$ , we show in SM.C [37] that the minimal travel time reads

$$t_{\min} = T_0 \left( \frac{x_0 \Gamma((3 + \alpha)/2)}{v T_0} \right)^{2/(1+\alpha)}, \quad (16)$$

which is a *decreasing* function of  $\alpha$ . In other words,  $t_{\min}$  is smaller in the superdiffusive regime than in the diffusive one, and that one is again less than for subdiffusion—a trend which is apparent in Fig. 4. Moreover, we observe that the approach of the mean fFPT to  $t_{\min}$  on an increase of  $N$  is fastest for superdiffusion and longest for subdiffusion, which agrees with physical intuition. The trend is reversed for  $x_0/(vT_0) < 1$ , when the target can

be reached in a single step (see SM.C [37]).

*Conclusions.* We revisited the biologically relevant problem of parallel search by  $N$  independent random searchers for an immobile target, a paradigmatic setting for extreme first-passage statistics in many applications. In the standard Brownian-motion framework, the mean fFPT decreases only logarithmically with  $N$  and formally vanishes as  $N \rightarrow \infty$ , implying both instantaneous arrival in the infinite- $N$  limit and a weak benefit from deploying multiple searchers. This framework further predicts subdiffusive dynamics to outperform normal diffusion—an artifact of the unphysical possibility of arbitrarily fast propagation.

Fixing this shortcoming, we formulated the search dynamics using dichotomous noise, leading to the telegrapher's equation with finite propagation speed and compact, time-dependent support of the position PDF. In this physically consistent setting, the mean fFPT converges, as  $N \rightarrow \infty$ , to a finite lower bound equal to the shortest possible, ballistic travel time. Remarkably, the convergence to this bound is exponentially fast in  $N$ , demonstrating a dramatic efficiency gain over Brownian search. From a biological perspective, it is thus meaningful to invest the energy to produce many searchers to substantially speed up underlying random search processes. For intermediate  $N$ , the convergence remains slow and mimics the familiar logarithmic behavior, thereby reconciling earlier results with finite-speed dynamics.

We extended our analysis to anomalous transport via the Riemann-Liouville dichotomous process. This yielded a clear hierarchy: superdiffusive search is most efficient, followed by diffusive scaling and then subdiffusion, in contrast to predictions from continuous-space fractional diffusion models.

Overall, our results show that imposing a finite propagation speed fundamentally alters the extreme first-passage behavior, resolves long-standing paradoxes of Brownian statistics, and identifies finite-velocity searchers as a superior strategy for rapid parallel target detection. Future research directions include determining the full fFPT distribution and extending the discrete-space approach developed in Ref. [50].

## ACKNOWLEDGMENTS

D.S.G acknowledges partial support by the Alexander von Humboldt Foundation within a Bessel Prize award. RM acknowledges grant ME 1535/22-1 from the German Science Foundation (DFG).

---

[1] M. Ptashne and A. Gann, *Genes and Signals* (Cold Spring Harbor Laboratory Press, 2002).  
[2] B. Alberts, A. Johnson, J. Lewis, M. Raff, K. Roberts,

and P. Walter, *Molecular Biology of the Cell* (Garland Science, 2002).  
[3] O. Bénichou, C. Loverdo, M. Moreau, and R. Voituriez,

Intermittent search strategies, *Rev. Mod. Phys.* **83**, 81-130 (2011).

[4] P. Hammar, P. Leroy, A. Mahmutovic, E. G. Marklund, O. G. Berg, and J. Elf, The lac repressor displays facilitated diffusion in living cells, *Science* **336**, 1595-1598 (2012).

[5] J. Ma, M. Do, M. A. Le Gros, C. S. Peskin, C. A. Larabell, Y. Mori, and S. A. Isaacson, Strong intracellular signal inactivation produces sharper and more robust signaling from cell membrane to nucleus, *PLoS Comp. Biol.* **16**, e1008356 (2020).

[6] M. Bauer and R. Metzler, In vivo facilitated diffusion model, *PLoS ONE* **8**, e53956 (2013).

[7] D. P. Snustad and M. J. Simmons, *Principles of Genetics* (Wiley, 2015).

[8] D. S. Grebenkov, R. Metzler and G. Oshanin (Eds.) *Target Search Problems* (Springer, Cham, CH, 2024).

[9] G. H. Weiss, K. E. Shuler and K. Lindenberg, Order statistics for first passage times in diffusion processes, *J. Stat. Phys.* **31**, 255-278 (1983).

[10] B. Meerson and S. Redner, Mortality, Redundancy, and Diversity in Stochastic Search, *Phys. Rev. Lett.* **114**, 198101 (2015).

[11] K. Reynaud, Z. Schuss, N. Rouach, and D. Holcman, Why so many sperm cells? *Comm. Integr. Biol.* **8**, e1017156 (2015).

[12] S. D. Lawley, Universal formula for extreme first passage statistics of diffusion, *Phys. Rev. E* **101**, 012413 (2020).

[13] S. D. Lawley, Distribution of extreme first passage times of diffusion, *J. Math. Biol.* **80**, 2301-2325 (2020).

[14] S. D. Lawley and J. B. Madrid, A Probabilistic Approach to Extreme Statistics of Brownian Escape Times in Dimensions 1, 2, and 3, *J. Nonlinear. Sci.* **30**, 1207-1227 (2020).

[15] J. B. Madrid and S. D. Lawley, Competition between slow and fast regimes for extreme first passage times of diffusion, *J. Phys. A: Math. Theor.* **53**, 335002 (2020).

[16] Z. Schuss, K. Basnayake, and D. Holcman, Redundancy principle and the role of extreme statistics in molecular and cellular biology, *Phys. Life Rev.* **28**, 52-79 (2019).

[17] D. S. Grebenkov, R. Metzler, and G. Oshanin, From single-particle stochastic kinetics to macroscopic reaction rates: fastest first-passage time of  $N$  random walkers, *New J. Phys.* **22**, 103004 (2020).

[18] D. S. Grebenkov, R. Metzler, and G. Oshanin, Search efficiency in the Adam-Delbrück reduction-of-dimensionality scenario versus direct diffusive search, *New J. Phys.* **24**, 083035 (2022).

[19] A. Godec and R. Metzler, Universal proximity effect in target search kinetics in the few encounter limit, *Phys. Rev. X* **6**, 041037 (2016).

[20] D. Grebenkov, R. Metzler, and G. Oshanin, Strong defocusing of molecular reaction times: geometry and reaction control, *Comm. Chem.* **1**, 96 (2018).

[21] R. Metzler, J.-H. Jeon, A. G. Cherstvy, and E. Barkai, Anomalous diffusion models and their properties: non-stationarity, non-ergodicity, and ageing at the centenary of single particle tracking, *Phys. Chem. Chem. Phys.* **16**, 24128 (2014).

[22] S. D. Lawley, Extreme statistics of anomalous subdiffusion following a fractional Fokker-Planck equation: subdiffusion is faster than normal diffusion, *J. Phys. A: Math. Theor.* **53**, 385005 (2020).

[23] P. Hänggi and P. Jung, Colored noise in dynamical systems, *Adv. Chem. Phys.* **89**, 239-326 (1995).

[24] I. Bena, Dichotomous Markov noise: exact results for out-of-equilibrium systems, *Int. J. Modern Phys. B* **20**, 2825-2888 (2006).

[25] T. Sandev, L. Kocarev, R. Metzler, and A. Chechkin, Stochastic dynamics with multiplicative dichotomic noise: Heterogeneous telegrapher's equation, anomalous crossovers and resetting, *Chaos, Solitons and Fractals* **165**, 112878 (2022).

[26] T. Herbeau, L. Pastur, P. Viot and G. Oshanin, Stochastic gyration driven by dichotomous noises, *J. Stat. Mech.* **2026**, 013205 (2026).

[27] C. R. Cattaneo, Sur une forme de l'équation de la chaleur éliminant le paradoxe d'une propagation instantanée (On a form of the heat equation eliminating the paradox of an instantaneous propagation), *C. R. Acad. Sci. Paris* **247**, 431 (1958).

[28] D. Jou, J. Casas-Vázquez, and G. Lebon, *Extended irreversible thermodynamics* (Springer, 2001).

[29] O. Bénichou, P. Illien, G. Oshanin, A. Sarracino, and R. Voituriez, Tracer diffusion in crowded narrow channels, *J. Phys.: Cond. Matter* **30**, 443001 (2018).

[30] J. Tailleur and M. E. Cates, Statistical mechanics of interacting run-and-tumble bacteria, *Phys. Rev. Lett.* **100**, 218103 (2008).

[31] A. B. Slowman, M. R. Evans and R. A. Blythe, Jamming and Attraction of Interacting Run-and-Tumble Random Walkers, *Phys. Rev. Lett.* **116**, 218101 (2016).

[32] Y. Zhao, C. Kurzthaler, N. Zhou, J. Schwarz-Linek, C. Devailly, J. Arlt, J.-D. Huang, W. C. K. Poon, T. Franosch, V. A. Martinez, and J. Tailleur, Quantitative characterization of run-and-tumble statistics in bulk bacterial suspensions, *Phys. Rev. E* **109**, 014612 (2024).

[33] D. S. Dean, S. M. Majumdar, and H. Schawe, Position distribution in a generalized run-and-tumble process, *Phys. Rev. E* **103**, 012130 (2021).

[34] K. Malakar, V. Jemseena, A. Kundu, K. Kumar, S. Sabhapandit, S. N. Majumdar, S. Redner, and A. Dhar, Steady state, relaxation and first-passage properties of a run-and-tumble particle in one-dimension, *J. Stat. Mech.* **2018**, 043215 (2018).

[35] F. Mori, P. Le Doussal, S. N. Majumdar, and G. Schehr, Universal survival probability for a d-dimensional run-and-tumble particle, *Phys. Rev. Lett.* **124**, 090603 (2020).

[36] Ü. Basu, S. Sabhapandit, and I. Santra, Target Search by Active Particles, in [8], pp. 463.

[37] Supplementary Information, <https://...>

[38] M. Yu, T. Castanheira Silva, A. van Opstal, S. Romeijn, H. A. Every, W. Jiskoot, G.-J. Witkamp and M. Ottens, The investigation of protein diffusion via H-cell microfluidics, *Biophys. J.* **116**, 595-609 (2019).

[39] see, e.g., P. Swietach, M. Zaniboni, A. K. Stewart, A. Rossini, K. W. Spitzer and R. D. Vaughan-Jones, Modelling intracellular H<sup>+</sup> ion diffusion, *Prog. Biophys. Mol. Biol.* **83**, 69-100 (2003).

[40] T. J. Lampo, S. Stylianidou, M. P. Backlund, P. A. Wiggins and A. J. Spakowitz, Cytoplasmic RNA-Protein Particles Exhibit Non-Gaussian Subdiffusive Behavior, *Biophys. J.* **112**, 532-542 (2017).

[41] C. Di Rienzo, V. Piazza, E. Gratton, F. Beltram and F. Cardarelli, Probing short-range protein Brownian motion in the cytoplasm of living cells, *Nat. Comm.* **5**, 5891 (2014).

- [42] O. Seksek, J. Biwersi and A. S. Verkman, Translational Diffusion of Macromolecule-sized Solutes in Cytoplasm and Nucleus, *J. Cell Biol.* **138**, 131-142 (1997).
- [43] J. D. Williams, An approximation to the probability integral, *Ann. Math. Statist.* **17**, 363-365 (1946).
- [44] G. Muñoz-Gil, G. Volpe, M. A. Garcia-March, E. Aghion, A. Argun, C. B. Hong, et al. Objective comparison of methods to decode anomalous diffusion, *Nat. Comm.* **12**, 6253 (2021).
- [45] H. Seckler and R. Metzler, Bayesian deep learning for error estimation in the analysis of anomalous diffusion, *Nat. Comm.* **13**, 6717 (2022).
- [46] B. B. Mandelbrot and J. W. Van Ness, Fractional Brownian motions, fractional noises and applications, *SIAM Rev.* **10**, 422-437 (1968).
- [47] Y. S. Mishura, *Stochastic calculus for fractional Brownian motion and related processes* (Springer-Verlag, Berlin, 2008).
- [48] O. Vilk, E. Aghion, T. Avgar, C. Beta, O. Nagel, A. Sabri, R. Sarfati, D. K. Schwartz, M. Weiss, D. Krapf, R. Nathan, R. Metzler, and M. Assaf, Unravelling the origins of anomalous diffusion: from molecules to migrating storks, *Phys. Rev. Res.* **4**, 033055 (2022).
- [49] W. Wang, Q. Wei, A. V. Chechkin, and R. Metzler, Different behaviors of diffusing diffusivity dynamics based on three different definitions of fractional Brownian motion, *Phys. Rev. E* **112**, 014108 (2025).
- [50] S. D. Lawley, Extreme first-passage times for random walks on networks, *Phys. Rev. E* **102**, 062118 (2020).

## Supplemental Material:

### Fastest first-passage time for multiple searchers with finite speed

Denis S. Grebenkov, Ralf Metzler, and Gleb Oshanin

In this Supplemental Material (SM), we provide additional details on the exact solution of the boundary value problem for a single particle, the calculation of the fastest first-passage time and its detailed properties, as well as on the simulation of anomalous-diffusion dynamics.

#### SM.A. EXACT SOLUTION FOR A SINGLE PARTICLE

For completeness, we compute the survival probability of a *single* particle on the positive semi-axis. This computation was performed in [34] (see also [35, 36]). Here we start from the same backward Fokker-Planck equations and provide an alternative computation, which yields the same results. Let  $S_{\pm}(t|x_0) = \mathbb{P}_{x_0, \pm}\{\tau > t\}$  denote the survival probability for a particle launched at  $x_0$  with the velocity  $\pm v$ . The switching between positive and negative velocities can be easily implemented into the backward Fokker-Planck equation:

$$\begin{aligned}\partial_t S_+(t|x_0) &= v \partial_{x_0} S_+(t|x_0) - \lambda S_+(t|x_0) + \lambda S_-(t|x_0), \\ \partial_t S_-(t|x_0) &= -v \partial_{x_0} S_-(t|x_0) - \lambda S_-(t|x_0) + \lambda S_+(t|x_0).\end{aligned}\quad (\text{S17})$$

The action of the time derivative onto the second equation reads

$$\begin{aligned}\partial_t^2 S_- &= -(\lambda + v \partial_{x_0}) \partial_t S_- + \lambda \partial_t S_+ \\ &= -(\lambda + v \partial_{x_0})[-v \partial_{x_0} S_- + \lambda(S_+ - S_-)] \\ &\quad + \lambda[v \partial_{x_0} S_+ - \lambda(S_+ - S_-)] \\ &= v^2 \partial_{x_0}^2 S_- - 2\lambda \partial_t S_-, \end{aligned}\quad (\text{S18})$$

i.e., one recovers the standard form of the telegrapher's equation (see, e.g., [24]),

$$(\partial_t^2 + 2\lambda \partial_t - v^2 \partial_{x_0}^2) S(t|x_0) = 0 \quad (x_0 > 0), \quad (\text{S19})$$

where we dropped the subscript minus. The initial condition for the survival probability is  $S(0|x_0) = 1$  for any  $x_0 > 0$ . In addition, one imposes the constraint  $\lim_{x_0 \rightarrow \infty} S(t|x_0) = 1$ , since a particle started from infinity cannot reach the origin in a finite time. As a particle started from  $x_0 = 0$  with a negative velocity immediately hits the origin, one has  $S(t|0) = 0$ . Finally, as we aim at dealing with the second-order (in time) equation (S19), we need to specify the initial value of the first time derivative, for which we take  $\partial_t S(0|x_0) = 0$ . This is a consequence of the initial condition  $S_{\pm}(0|x_0) = 1$  and of the above backward Fokker-Planck equation for  $S_-(t|x_0)$ .

The Laplace transform of Eq. (S19) yields

$$\begin{aligned}(p^2 + 2\lambda p - v^2 \partial_{x_0}^2) \tilde{S}(p|x_0) \\ = (2\lambda + p) S(0|x_0) + S'(0|x_0) = 2\lambda + p\end{aligned}\quad (x_0 > 0), \quad (\text{S20})$$

where

$$\tilde{S}(p|x_0) = \int_0^\infty dt e^{-pt} S(t|x_0) \quad (p > 0). \quad (\text{S21})$$

Its solution on the positive semi-axis reads

$$\tilde{S}(p|x_0) = \frac{1}{p} - \frac{1}{p} e^{-\sqrt{p^2 + 2\lambda p} x_0/v}, \quad (\text{S22})$$

whereas its inverse Laplace transform is given by

$$\begin{aligned}S(t|x) &= 1 - \Theta(t - x_0/v) \left[ e^{-\lambda x_0/v} \right. \\ &\quad \left. + \lambda x_0/v \int_{\lambda x_0/v}^{xt} dz \frac{e^{-z} I_1(\sqrt{z^2 - (\lambda x_0/v)^2})}{\sqrt{z^2 - (\lambda x_0/v)^2}} \right], \end{aligned}\quad (\text{S23})$$

where  $I_{\nu}(z)$  is the modified Bessel function of the first kind and  $\Theta(z)$  is the Heaviside step function:  $\Theta(z) = 1$  for  $z > 0$  and 0 otherwise. One sees that the survival probability is strictly unity for  $t < x_0/v$ , and then it exhibits a jump  $e^{-\lambda x_0/v}$ , which corresponds to the possibility to reach the target by a single displacement. The negative time derivative of  $S(t|x_0)$  gives the FPT-PDF

$$\begin{aligned}H(t|x_0) &= \delta(t - x_0/v) e^{-\lambda x_0/v} + \Theta(t - x_0/v) (x_0/v) \lambda \\ &\quad \times \frac{e^{-\lambda t} I_1(\lambda \sqrt{t^2 - (x_0/v)^2})}{\sqrt{t^2 - (x_0/v)^2}}.\end{aligned}\quad (\text{S24})$$

The jump in the survival probability leads to a Dirac- $\delta$  distribution in the FPT-PDF at  $t = x_0/v$ . At long times, we use  $I_{\nu}(z) \simeq e^z / \sqrt{2\pi z}$  to show that this PDF approaches the Lévy-Smirnov density with the standard heavy tail,

$$H(t|x_0) \simeq \frac{x_0 e^{-x_0^2/(4Dt)}}{\sqrt{4\pi Dt^3}} \propto t^{-3/2} \quad (t \rightarrow \infty), \quad (\text{S25})$$

where  $D = v^2/(2\lambda)$  is the effective diffusion coefficient. In particular, the mean FPT is infinite, as for ordinary diffusion on the halfline.

It is convenient to express the above results in terms of the parameters  $\gamma = \lambda x_0/v$  and  $t_{\min} = x_0/v$  by setting  $\lambda = v^2/(2D) = \gamma/t_{\min}$ . The survival probability from Eq. (S23) then becomes

$$S(t|x_0) = 1 - \Theta(t - t_{\min}) \left[ e^{-\gamma} + \gamma \int_1^{t/t_{\min}} dz \frac{e^{-\gamma z} I_1(\gamma \sqrt{z^2 - 1})}{\sqrt{z^2 - 1}} \right]. \quad (\text{S26})$$

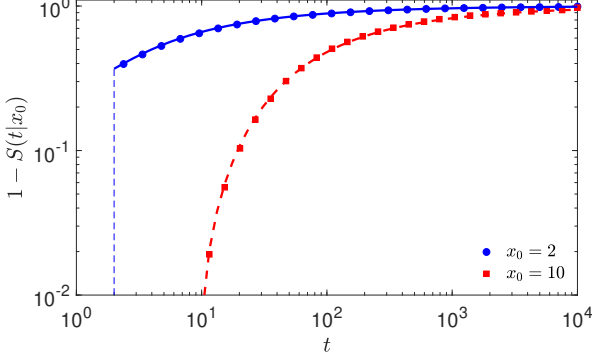


FIG. S5. CDF of the FPT to the absorbing origin on the halfline, with  $v = 1$  and  $\lambda = 0.5$  such that  $D = 1$ , and two values of  $x_0$  as shown in the caption. The solid line represents Eq. (S23), filled symbols show the empirical CDF from Monte Carlo simulations with  $M = 10^4$  particles.

Since the survival probability vanishes at infinity,  $S(\infty|x_0) = 0$ , we get the identity

$$\int_1^\infty dz \frac{e^{-\gamma z} I_1(\gamma \sqrt{z^2 - 1})}{\sqrt{z^2 - 1}} = \frac{1 - e^{-\gamma}}{\gamma} \quad (\gamma > 0). \quad (\text{S27})$$

Figure S5 illustrates the cumulative distribution function (CDF)  $1 - S(t|x_0)$ , either given by Eq. (S23), or estimated directly from Monte Carlo simulations (see Sec. SM.C). We observe excellent agreement for both  $x_0 = 2$  and  $x_0 = 10$ . Remarkably, the macroscopic description provided by the telegrapher's equation, which a priori should require a sufficiently large number of jumps (that corresponds to large  $x_0$  and  $t$ ), is so accurate even for moderate  $x_0$ .

### SM.B. FASTEST FIRST-PASSAGE TIME

This Section presents the mathematical details for our main results on the ffPT  $\mathcal{T}_N = \min\{\tau_1, \dots, \tau_N\}$  among  $N$  independent particles started from the same point  $x_0$ . The probability law of this random variable is

$$\mathbb{P}_{x_0}\{\mathcal{T}_N > t\} = S_N(t|x_0) = [S(t|x_0)]^N, \quad (\text{S28})$$

whereas its PDF is given by

$$H_N(t|x_0) = N H(t|x_0) [S(t|x_0)]^{N-1}, \quad (\text{S29})$$

where  $S(t|x_0)$  and  $H(t|x_0)$  are from Eqs. (S23) and (S24), respectively.

According to Eq. (S25), one has  $S(t|x) \simeq \sqrt{2T/(\pi t)}$  at long times  $t \gg T = x_0^2/(2D)$  such that

$$H_N(t|x_0) \simeq N \frac{2^{3N/2-1} T^{N/2}}{\pi^{N/2} t^{1+N/2}} \quad (t \rightarrow \infty). \quad (\text{S30})$$

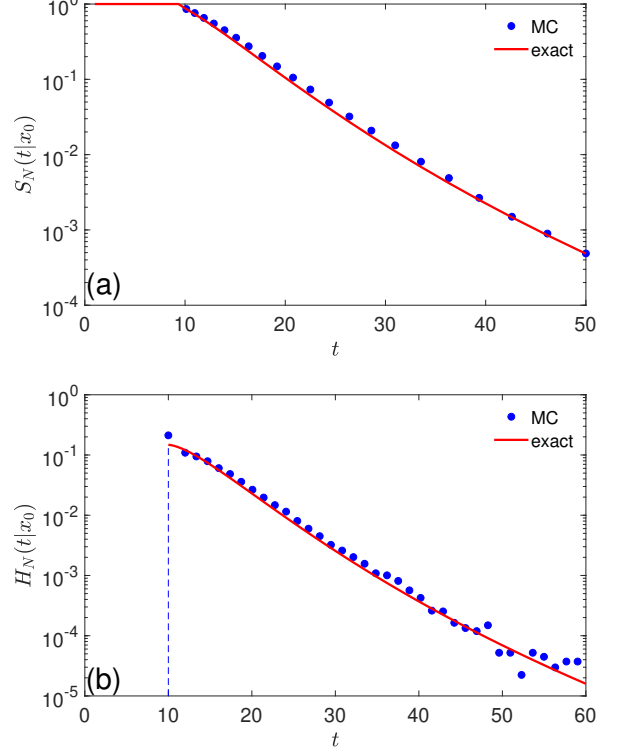


FIG. S6. Survival probability (a) and PDF (b) of the fastest FPT among  $N = 20$  particles on the halfline with absorbing origin,  $v = 1$ , and  $\lambda = 0.5$  such that  $D = 1$ , and  $x_0 = 10$ . Solid lines show the exact relations (S28) and (S29), with  $S(t|x_0)$  and  $H(t|x_0)$  given by Eqs. (S23) and (S24), whereas filled circles represent the empirical results from Monte Carlo simulations with  $M = 10^5$  particles.

Panel (a) of Fig. S6 compares the survival probability  $S_N(t|x_0)$  for  $N = 20$  independent particles with its empirical estimate, whereas panel (b) shows the PDF. Figure S7 compares the PDFs for the three values  $N = 1, 10$ , and  $20$ . In all cases, we observe the long-time asymptotic behavior (S30).

In the following, we focus on the mean ffPT and its variance and their asymptotic behavior for large  $N$ .

### 1. Mean ffPT

Let us now consider the mean ffPT

$$\overline{\mathcal{T}_N} = \int_0^\infty dt [S(t|x_0)]^N. \quad (\text{S31})$$

According to the asymptotic behavior (S25), this integral diverges for  $N = 1$  and  $N = 2$ , as in the case of ordinary diffusion. The following analysis is therefore restricted to  $N \geq 3$ .

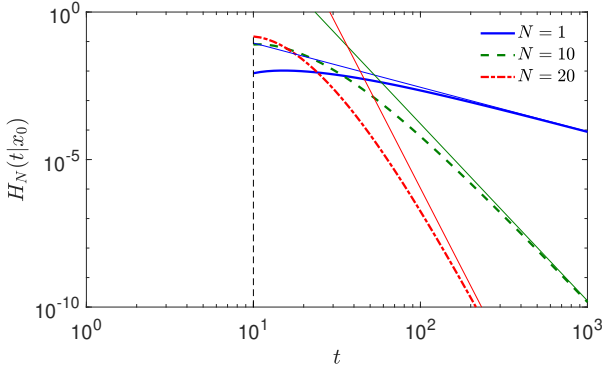


FIG. S7. PDF  $H_N(t|x_0)$  of the fFPT among  $N$  particles on the halfline with absorbing origin,  $v = 1$ , and  $\lambda = 0.5$ , such that  $D = 1$ , and  $x_0 = 10$ . Thick lines show the exact form (S29), whereas thin lines represent the long-time asymptotic behavior (S30). The minimal value of the fFPT is  $t_{\min} = x_0/v = 10$  (shown by the vertical dashed line), i.e., the PDF is strictly 0 for any  $t < t_{\min}$ .

The structure of  $S(t|x)$  in Eq. (S23) implies that

$$\overline{T_N} = \frac{x_0}{v} (1 + B_{N,\gamma}), \quad (\text{S32})$$

where

$$B_{N,\gamma} = \int_1^\infty dy [f_\gamma(y)]^N, \quad (\text{S33})$$

with

$$\begin{aligned} f_\gamma(y) &= 1 - e^{-\gamma} - \gamma \int_1^y dz \frac{e^{-\gamma z} I_1(\gamma \sqrt{z^2 - 1})}{\sqrt{z^2 - 1}} \\ &= \gamma \int_y^\infty dz \frac{e^{-\gamma z} I_1(\gamma \sqrt{z^2 - 1})}{\sqrt{z^2 - 1}} \quad (y \geq 1), \end{aligned} \quad (\text{S34})$$

where we used Eq. (S27) for the second equality. Changing the integration variable  $z = \cosh z'$ , one gets Eq. (7b) in the main text.

## 2. Asymptotic behavior at large $N$

In this Section, we inspect the asymptotic behavior of  $B_{N,\gamma}$  in the limit  $N \rightarrow \infty$  for fixed  $\gamma$ . For this purpose, we rewrite Eq. (S33) in the form

$$B_{N,\gamma} = \int_1^\infty dy e^{N \ln(f_\gamma(y))}. \quad (\text{S35})$$

Since  $\ln(f_\gamma(y))$  with  $f_\gamma(y)$  defined in Eq. (S34) is a monotonically decreasing function of  $y$ , the above integral is

supported by the behavior of  $\ln(f_\gamma(y))$  in the close proximity of  $y = 1$ . Using its Taylor expansion near  $y = 1$ ,

$$\ln(f_\gamma(y)) = \ln(1 - e^{-\gamma}) - \frac{\gamma^2(y-1)}{2(e^\gamma - 1)} + \mathcal{O}((y-1)^2), \quad (\text{S36})$$

we find to leading order in the limit  $N \rightarrow \infty$  that

$$B_{N,\gamma} \approx \frac{2(e^\gamma - 1)}{\gamma^2 N} (1 - e^{-\gamma})^N. \quad (\text{S37})$$

Rewriting this expression formally we get our asymptotic result in Eq. (9).

One sees that the mean fFPT approaches a constant limit  $x_0/v$  (the minimal value of the fFPT), and this approach is *exponentially fast* with  $N$ :  $T_N - x_0/v \propto e^{-N/N_\gamma}$ , where  $N_\gamma$  is given by Eq. (8). In particular, in the limit of small  $\gamma$ , one has  $N_\gamma \approx 1/\ln(1/\gamma) \rightarrow 0$ , i.e., the decay is very fast. In the opposite limit of large  $\gamma$ , one gets  $N_\gamma \approx e^\gamma \rightarrow +\infty$ , i.e., the decay becomes much slower, still being exponential for any fixed  $\gamma$ . Since  $N_\gamma$  grows exponentially fast with  $\gamma$ , one may need to consider very large  $N$  to observe the exponential decay for large  $\gamma$ .

## 3. Intermediate regime

We seek an accurate uniform approximation of  $f_\gamma(y)$  in Eq. (7b) for all  $y$  away from the point  $y = 1$ , which will permit us to describe the behavior for  $N$  in the interval  $3 \leq N \ll N_\gamma$ . To this end, it is convenient to change the integration variable  $z$  as  $u = \exp(-z)$ , which leads to

$$f_\gamma(y) = \gamma \int_0^b \frac{du}{u} \exp\left(-\frac{\gamma}{2}\left(\frac{1}{u} + u\right)\right) I_1\left(\frac{\gamma}{2}\left(\frac{1}{u} - u\right)\right), \quad (\text{S38})$$

where  $b = e^{-\text{arccosh}(y)} = 1/(y + \sqrt{y^2 - 1})$ . The upper limit of integration is less than unity, and the dominant contribution to the integral comes from the region in the vicinity of  $u = 0$ . Supposing that  $\gamma$  is bounded away from zero, we have

$$\frac{\gamma}{2}\left(\frac{1}{u} - u\right) \gg 1, \quad (\text{S39})$$

which allows us to use the large-argument expansion for the modified Bessel function of the first kind,

$$I_1\left(\frac{\gamma}{2}\left(\frac{1}{u} - u\right)\right) \approx \sqrt{\frac{u}{\pi\gamma}} \exp\left(\frac{\gamma}{2}\left(\frac{1}{u} - u\right)\right). \quad (\text{S40})$$

This yields

$$f_\gamma(y) \approx \sqrt{\gamma} \int_0^b \frac{du}{\sqrt{u}} \exp\left(-\frac{\gamma}{2u}\right) = \text{erf}\left(\sqrt{\gamma b}\right), \quad (\text{S41})$$

where  $\text{erf}(x)$  is the error function. The approximation in Eq. (S41) describes  $f_\gamma(y)$  very well for all  $y$  sufficiently away from  $y = 1$ , and the agreement improves

as  $\gamma$  increases. Indeed, at the "worst point"  $y = 1$ , the exact value is  $f_\gamma(1) = 1 - e^{-\gamma}$ , whereas Eq. (S41) yields  $f_\gamma(1) = \text{erf}(\sqrt{\gamma})$ , which matches the exact result only in the formal limit  $\gamma = \infty$ . In this regime, setting  $x = \sqrt{b} = (y + \sqrt{y^2 - 1})^{-1/2}$  (and thus  $y = (x^2 + x^{-2})/2$ ), the relaxation function  $B_{N,\gamma}$  in Eq. (7) can be written as

$$B_{N,\gamma} \approx \int_0^1 dx \frac{1-x^4}{x^3} [\text{erf}(\sqrt{\gamma}x)]^N \quad (N \geq 3), \quad (\text{S42})$$

representing a very accurate approximation to the actual value of  $B_{N,\gamma}$  for moderate  $N$ , such that  $Ne^{-\gamma} < 1$ , for which the integral in Eq. (7) is supported on values of  $y$  that remain away from  $y = 1$ .

The integral on the right-hand-side of Eq. (S42) can be estimated as follows: a very tight upper bound on  $\text{erf}(x)$  for any value of  $x \geq 0$  (the error not exceeding 1 percent) is given by [43]

$$\text{erf}(x) \leq \sqrt{1 - \exp\left(-\frac{4x^2}{\pi}\right)}. \quad (\text{S43})$$

Assuming for simplicity that  $N$  is even, we bound the integral on the right-hand-side of Eq. (S42) from above as

$$\begin{aligned} \int_0^1 dx \frac{1-x^4}{x^3} [\text{erf}(\sqrt{\gamma}x)]^N &\leq \lim_{\epsilon \rightarrow 0} \left\{ \sum_{j=0}^{N/2} (-1)^j \binom{N/2}{j} \right. \\ &\quad \times \int_\epsilon^1 dx \frac{1-x^4}{x^3} \exp\left(-\frac{4\gamma j}{\pi} x^2\right) \Big\} \\ &= \lim_{\epsilon \rightarrow 0} \left[ \frac{1}{2\epsilon^2} - 1 + \frac{\epsilon^2}{2} + \sum_{j=1}^{N/2} (-1)^j \binom{N/2}{j} \Phi_j(\epsilon) \right], \end{aligned} \quad (\text{S44})$$

where

$$\begin{aligned} \Phi_j(\epsilon) &= \frac{\pi}{8\gamma j} \left( \exp\left(-\frac{4\gamma j}{\pi}\right) - \exp\left(-\frac{4\gamma j \epsilon^2}{\pi}\right) \right) \\ &\quad - \frac{1}{2} \exp\left(-\frac{4\gamma j}{\pi}\right) + \frac{1}{2\epsilon^2} \exp\left(-\frac{4\gamma j \epsilon^2}{\pi}\right) \\ &\quad - \frac{2\gamma j}{\pi} \text{Ei}\left(-\frac{4\gamma j}{\pi}\right) + \frac{2\gamma j}{\pi} \text{Ei}\left(-\frac{4\gamma j \epsilon^2}{\pi}\right), \end{aligned} \quad (\text{S45})$$

with  $\text{Ei}(-z)$  denoting the exponential integral

$$\text{Ei}(-z) = - \int_z^\infty dx \frac{\exp(-x)}{x}. \quad (\text{S46})$$

Further on, we single out the part of  $\Phi_j(\epsilon)$  dependent on  $\epsilon$  and expand it into a Taylor series in powers of  $\epsilon$ . Summing it up over  $j$  we observe that the singular terms cancel each other when  $N \geq 3$ , as they should—indeed,

the integral in Eq. (S42) exists for  $\epsilon = 0$  once  $N > 2$ . Assuming next that  $\gamma$  is sufficiently large such that all terms containing  $\exp(-\gamma)$  can be safely neglected, as compared to the terms containing only powers of  $\gamma$ , we get our estimate in Eq. (11), where we used the following representation of the harmonic number

$$H_n = \sum_{j=1}^n \frac{(-1)^{j+1}}{j} \binom{n}{j} = \sum_{j=1}^n \frac{1}{j}, \quad (\text{S47})$$

as well as the binomial identity

$$\sum_{j=1}^n (-1)^j j \binom{n}{j} = 0. \quad (\text{S48})$$

Note that the harmonic number admits the large- $n$  expansion

$$H_n = \ln n + C + \frac{1}{2n} - \frac{1}{12n^2} + \mathcal{O}(n^{-4}), \quad (\text{S49})$$

where  $C \approx 0.5772$  is the Euler constant.

To get the asymptotic behavior of the coefficients  $S_n$  from Eq. (12), we first use the identity

$$\ln(j) = \int_0^\infty du \frac{e^{-u} - e^{-ju}}{u} \quad (j \geq 1) \quad (\text{S50})$$

to deduce two equivalent integral representations of  $S_n$ , which are suitable for its computation for large  $n$ ,

$$S_n = n \int_0^\infty du \frac{e^{-u}(1 - e^{-u})^{n-1}}{u} = n \int_0^1 dz \frac{(1 - z)^{n-1}}{-\ln z}. \quad (\text{S51})$$

Setting  $v = nz$  and expanding  $1/(-\ln z) = 1/(\ln n - \ln v)$  into a geometric series, we get the asymptotic behavior of  $S_n$  at large  $n$ ,

$$S_n = \sum_{k \geq 0} \frac{m_k}{(\ln n)^k}, \quad m_k = \int_0^\infty dv e^{-v} (\ln v)^k. \quad (\text{S52})$$

In particular, one has  $m_0 = 1$ ,  $m_1 = -C$ ,  $m_2 = C^2 + \pi^2/6$ , etc.

#### 4. Diffusion limit

The diffusion limit corresponds to  $v \rightarrow \infty$  and  $\lambda \rightarrow \infty$  with  $D = v^2/(2\lambda)$  being fixed. In this case, one has  $\gamma = x_0 v/(2D) \rightarrow \infty$ .

First, we check that the survival probability  $S(t|x_0)$  approaches the expected limit of ordinary diffusion as  $\gamma \rightarrow \infty$ . In fact, the Heaviside function in Eq. (S26) can be replaced by unity, whereas  $e^{-\gamma}$  vanishes. Using the asymptotic behavior of the modified Bessel function,  $I_1(z) \simeq e^z/\sqrt{2\pi z}$  as  $z \rightarrow \infty$ , we can approximate the integral in Eq. (S26) to get

$$\begin{aligned}
S(t|x_0) &\approx 1 - \gamma \int_1^{\gamma t/T} dz \frac{e^{-\gamma z + \gamma \sqrt{z^2 - 1}}}{(z^2 - 1)^{3/4} \sqrt{2\pi\gamma}} \approx 1 - \frac{\sqrt{\gamma}}{\sqrt{2\pi}} \int_1^{\gamma t/T} dz \frac{e^{-\gamma/(2z)}}{(z^2 - 1)^{3/4}} \\
&= 1 - \frac{\sqrt{\gamma/2}}{\sqrt{\pi}} \int_{2/\gamma}^{2t/T} dz \frac{e^{-1/z}(\gamma/2)}{(\gamma^2 z^2/4 - 1)^{3/4}} \approx 1 - \frac{\sqrt{\gamma/2}}{\sqrt{\pi}} \int_0^{2t/T} dz \frac{e^{-1/z}(\gamma/2)}{(\gamma/2)^{3/2} z^{3/2}} \\
&= 1 - \frac{1}{\sqrt{\pi}} \int_0^{2t/T} dz \frac{e^{-1/z}}{z^{3/2}} = 1 - \frac{2}{\sqrt{\pi}} \int_{\sqrt{T/(2t)}}^{\infty} dz e^{-z^2} = \text{erf}(\sqrt{T/(2t)}), \tag{S53}
\end{aligned}$$

where  $T = x_0^2/(2D)$ . In other words, we recover the expected diffusion limit,

$$S(t|x_0) \rightarrow \text{erf}(x_0/\sqrt{4Dt}) \quad (\gamma \rightarrow \infty). \tag{S54}$$

Next, we turn to the analysis of the mean ffPFT. Substituting  $v = 2D\gamma/x_0$  into Eq. (S32), we first rewrite it as

$$\overline{\mathcal{T}_N} = T \frac{1 + B_{N,\gamma}}{\gamma}. \tag{S55}$$

In order to evaluate the limit  $\gamma \rightarrow \infty$  (for fixed  $N$ ), we use the approximate representation (S42). Substituting  $z = \sqrt{\gamma}x$ , we have

$$\frac{B_{N,\gamma}}{\gamma} \approx \int_0^{\sqrt{\gamma}} \frac{dz}{z^3} [\text{erf}(z)]^N - \frac{1}{\gamma^2} \int_0^{\sqrt{\gamma}} dz z [\text{erf}(z)]^N. \tag{S56}$$

The second integral vanishes as  $\gamma \rightarrow \infty$ , whereas the first integral approaches the well-defined limit

$$\lim_{\gamma \rightarrow \infty} \frac{B_{N,\gamma}}{\gamma} \approx \int_0^{\infty} \frac{dz}{z^3} [\text{erf}(z)]^N. \tag{S57}$$

Its large- $N$  asymptotic behavior follows from the analysis of the mean ffPFT for ordinary diffusion,

$$\int_0^{\infty} dt [\text{erf}(x_0/\sqrt{4Dt})]^N = \frac{x_0^2}{2D} \int_0^{\infty} dz \frac{dz}{z^3} [\text{erf}(z)]^N, \tag{S58}$$

so that

$$\int_0^{\infty} dz \frac{dz}{z^3} [\text{erf}(z)]^N \simeq \frac{1}{2 \ln N} + \mathcal{O}([\ln(N)]^{-2}). \tag{S59}$$

We therefore recover the leading-order term of the mean ffPFT in the diffusion limit.

## 5. Variance and higher-order moments of the ffPFT

According to Eq. (S26), the  $k$ th-order moment of the ffPFT is

$$\begin{aligned}
\overline{\mathcal{T}_N^k} &= k \int_0^{\infty} dt t^{k-1} [S(t|x_0)]^N \\
&= t_{\min}^k \left\{ 1 + k \int_1^{\infty} dy y^{k-1} [f_{\gamma}(y)]^N \right\}, \tag{S60}
\end{aligned}$$

where the function  $f_{\gamma}(y)$  is defined in Eq. (S34), and  $t_{\min} = x_0/v$ . In particular, the variance reads

$$\frac{\text{var}\{\mathcal{T}_N\}}{t_{\min}^2} = 2 \int_1^{\infty} dy (y-1) [f_{\gamma}(y)]^N - \left( \int_1^{\infty} dy [f_{\gamma}(y)]^N \right)^2. \tag{S61}$$

In the limit  $N \rightarrow \infty$  with fixed  $\gamma$ , one employs again the Taylor expansion (S36) to get

$$\frac{\text{var}\{\mathcal{T}_N\}}{t_{\min}^2} \simeq (1 - e^{-\gamma})^N \frac{4(e^{\gamma} - 1)^2}{\gamma^4 N^2} (2 - (1 - e^{-\gamma})^N), \tag{S62}$$

which is valid for  $N \gg N_{\gamma}$ . While the mean ffPFT approaches its minimal value  $t_{\min}$ , the variance vanishes exponentially fast, i.e., the PDF of the ffPFT becomes concentrated near  $t_{\min}$ .

In the intermediate regime  $3 \leq N \ll N_{\gamma}$ , one can adapt the asymptotic technique from Sec. SM.B 3 to analyze the variance. However, we skip this analysis and employ numerical computation of the integrals in Eq. (S61) to illustrate its behavior (see Fig. 3).

## SM.C. SIMULATIONS FOR ANOMALOUS DIFFUSION

In this Section, we describe Monte Carlo simulations for anomalous diffusion governed by dichotomous noise. As the particles move independently from each other, we restrict the construction to a single particle trajectory, omitting the index  $k$  enumerating different particles.

The dichotomous noise process can be formally defined in terms of independent identically distributed random variables  $\delta_i$ , obeying the exponential law with the mean  $1/\lambda$ ,

$$\begin{aligned}\eta(t) &= v(-1)^{n(t)+n_0}, \\ n(t) &= \min \left\{ n > 0 : \sum_{i=1}^n \delta_i \geq t \right\},\end{aligned}\quad (\text{S63})$$

where  $n_0$  characterizes the choice of the sign in the first step (in our simulations, we set  $n_0 = 1$  to start with the negative sign). Substituting Eq. (S63) into Eq. (5), one gets

$$\begin{aligned}x(t) &= x_0 + \frac{vT_0^{1-\beta}(-1)^{n_0}}{\Gamma(\beta+1)} \\ &\times \left\{ t^\beta + 2 \sum_{i=1}^{n(t)} (-1)^i (t - (\delta_1 + \dots + \delta_i))^\beta \right\},\end{aligned}\quad (\text{S64})$$

where we introduced a shortcut notation  $\beta = (\alpha+1)/2$ . For practical purposes, we aim at evaluating  $x(t)$  at times  $t_i = \delta_1 + \dots + \delta_i$ . Note that  $n(t_n) = n$  by construction such that

$$\begin{aligned}x(t_n) &= x_0 + \frac{vT_0^{1-\beta}(-1)^{n_0}}{\Gamma(\beta+1)} \left\{ t_n^\beta + 2 \sum_{i=1}^{n-1} (-1)^i (t_n - t_i)^\beta \right\}, \\ x(t_1) &= x_0 + \frac{vT_0^{1-\beta}(-1)^{n_0}}{\Gamma(\beta+1)} t_1^\beta.\end{aligned}\quad (\text{S65})$$

In the case of ordinary diffusion ( $\alpha = 1$ ), we have  $\beta = 1$  and obtain

$$x(t_n) = x(t_{n-1}) + v\delta_n(-1)^{n-1+n_0} \quad (n = 1, 2, \dots),\quad (\text{S66})$$

with  $x(0) = x_0$ , as expected. This recurrence relation is used for Monte Carlo simulations in the diffusive regime

( $\alpha = 1$ ). In fact, for  $N$  particles, we advance their positions in parallel by generating waiting times. When one particle has crossed the target (i.e.,  $x(t_n) < 0$ ), the simulation is stopped, and the crossing time is evaluated. We mention a potential drawback of this simulation: if one particle is advanced by large  $\delta_n$ , another particle might cross the origin earlier. However, as the probability of getting abnormally large  $\delta_n$  is exponentially small, the induced error is small. We checked that it was actually negligible.

The situation is different for the anomalous case ( $\alpha \neq 1$ ). In fact, for each step  $t_n$ , one needs to re-evaluate the sum in Eq. (S65) that would result in much slower simulations. Once the simulation is stopped when  $x(t_n) < 0$ , the crossing time  $t_c$ , lying between  $t_{n-1}$  and  $t_n$ , is evaluated by solving numerically the equation  $x(t_c) = 0$ , where  $x(t)$  is given by Eq. (S64) with  $n(t) = n - 1$ .

It is worth noting that the minimal time to reach the target for a single particle corresponds to a single move, so that  $x(t) = x_0 - vT_0^{1-\beta}t^\beta/\Gamma(\beta+1)$ , from which our Eq. (16) follows. When  $x_0/(vT_0)$  is large enough,  $t_{\min}$  is a monotonously decreasing function of  $\beta$  (or  $\alpha$ ), as intuitively expected; in particular, superdiffusion allows to reach the target *faster* than subdiffusion. However, if  $x_0/(vT_0) \lesssim 1$ , the opposite trend occurs, i.e.,  $t_{\min}$  monotonously increases with  $\alpha$ . Here we thus return to the counter-intuitive situation when superdiffusion may look less efficient than subdiffusion. We emphasize however, that this "paradox" is rather artificial. In fact, when  $x^2(t) \sim t^\alpha$ , the MSD with a larger  $\alpha$  grows faster only at long times; in turn, it grows slower at short times. As the first-passage time is determined by short times, we are in the seemingly "paradoxical" setting when superdiffusion is less efficient than subdiffusion.